Catalysis Science & Technology

Accepted Manuscript

This article can be cited before page numbers have been issued, to do this please use: Y. Samoilichenko, V. Kondratenko, M. Ezernitskaya, K. Lyssenko, A. S. Peregudov, V. Khrustalev, V. I. Maleev, M. Margarita Moskalenko, M. North, A. Tsaloev, Z. Gugkaeva and Y. N. Belokon, *Catal. Sci. Technol.*, 2016, DOI: 10.1039/C6CY01697A.

ROYAL SOCIETY OF CHEMISTRY

rsc.li/catalysis

View Article Online
DOI: 10.1039/C6CY01697A

Journal Name

ARTICLE

A mechanistic study of the Lewis acid-Brønsted base-Brønsted acid catalysed asymmetric Michael addition of diethyl malonate to cyclohexenone

Received 00th January 20xx,
Accepted 00th January 20xx

DOI: 10.1039/x0xx00000x

www.rsc.org/

Yuri Samoilichenko,[a,b] Veronica Kondratenko,[a,c] Mariam Ezernitskaya,[a] Konstantin Lyssenko,[a] Alexander Peregudov,[a], Victor Khrustalev,[a,d] Victor Maleev,[a] Margarita Moskalenko,[a] Michael North,[e] Alan Tsaloev,[f] Zalina T. Gugkaeva,[a] and Yuri Belokon[a*]

The Michael addition of diethyl malonate (***M**ichael **D**onor*, ***MD***) to cyclohexenone (***M**ichael **A**cceptor*, ***MA***) catalysed by the mono-lithium salt of (*S*)- or (*R*)-BIMBOL in dichloromethane is shown to exhibit biomimetic behavior. A combination of kinetics, spectroscopic studies, synthesis of catalyst analogues, inhibition studies and DFT calculations are used to show that the catalyst activates both components of the reaction and uses a chain of proton transfers to facilitate the deprotonation of diethyl malonate. The initial reaction rate was first order relative to both ***MA*** and ***MD*** and 0.5 order relative to the catalyst, indicating that an equilibrium exists between monomeric and dimeric forms of the catalyst, with the dimer predominanting, but only the monomeric form being catalytically active. This was supported by DOSY ^{1}H NMR experiments. The importance of the Lewis acidic lithium cation in the catalytic step was established by complete inhibition of the reaction by lithium complexing agents. The importance of the number of OH-groups and their relative intramolecular orientation and acidities in the polyol catalyst was shown by studying the relative catalytic activities of catalyst analogues. DFT calculations allowed the relative energies and structures of the likely intermediates on the reaction coordinate to be calculated and indicated that the ionisation of ***MD*** was facilitated due to the Lewis acidity of the lithium cation and hydrogen bond formation between deprotonated ***MD*** (***MD*$^{-1}$**) and the OH groups of the BIMBOL moiety.

Introduction

Asymmetric catalysis using synthetic catalysts has advanced enormously over the last 25 years. Metal catalysed reactions are well established[1] and asymmetric organocatalysis has blossomed over the last 15 years,[2,3] with chiral Brønsted acid and hydrogen bond donor catalysis being amongst the most recent developments.[3] Despite these impressive advances, synthetic catalysts still struggle to match the levels of activity and asymmetric induction achieved with enzymes. This is due to the presence of multiple, exquisitely orientated, functional groups within the active site of enzymes which facilitates both simultaneous activation of both reaction components; and intramolecular proton transfer to lower the energy of transition states between reaction intermediates.[4] In this paper we show that a chiral synthetic catalyst containing both metal-based and non-metal based catalytic groups facilitates both intramolecular proton transfer and reactant activation in a biomimetic way.

The introduction of basic groups into catalysts, alongside hydrogen bonding functions, results in highly efficient bifunctional chiral catalysts capable of simultaneous activation of both nucleophilic and electrophilic components of heterolytic reactions.[3,5] The most popular catalytic motif of this type is represented by amine-thiourea organocatalysts.[5] Recently, the combined use of metal-based and organocatalysts has been shown to catalyse tandem processes.[6] As a result of these discoveries the established mechanisms of asymmetric catalysts have been re-evaluated and some well accepted cases of Lewis acid catalysis have been shown to originate from hidden Brønsted acid catalysis[7] occurring via Lewis acid activated Brønsted acid catalysis.[8]

Another emerging multifunctional catalytic system for asymmetric C-C and C-H bond formation is exemplified by chiral alkali binaphtholate salts.[9] These catalysts contain a Lewis acidic site, Brønsted basic and Brønsted acidic sites. The corresponding alkali metal salts of TADDOLs and bis-TADDOLs were also efficient in promoting asymmetric carbon–carbon

[a] *A.N. Nesmeyanov Institute of Organoelement Compounds, Russian Academy of Sciences, 28 Vavilov Street, Moscow 119991, Russian Federation. yubel@ineos.ac.ru; Fax: +7 (495) 135 5085.*
[b] *Present adress, Biotech Industry Ltd, 1 Leninskye Gory, Moscow 119992, Russian Federation.*
[c] *Present adress, Drugs Technology, 2a Rabochaya Street, Khimki, Moscow Region, 141400, Russian Federation.*
[d] *Peoples' Friendship University of Russia, 6 Miklukho-Maklay Street, Moscow 117198, Russian Federation.*
[e] *Green Chemistry Centre of Excellence, Department of Chemistry, The University of York, Heslington, York, YO10 5DD (UK).*
[f] *Chemical Diversity Research Institute, 2a Rabochaya Street, Khimki, Moscow Region, 141400, Russian Federation.*

†Electronic Supplementary Information (ESI) available: [Experimental, X-ray and computational details, NMR spectra and HPLC traces.]. See DOI: 10.1039/x0xx00000x

View Article Online
DOI: 10.1039/C6CY01697A

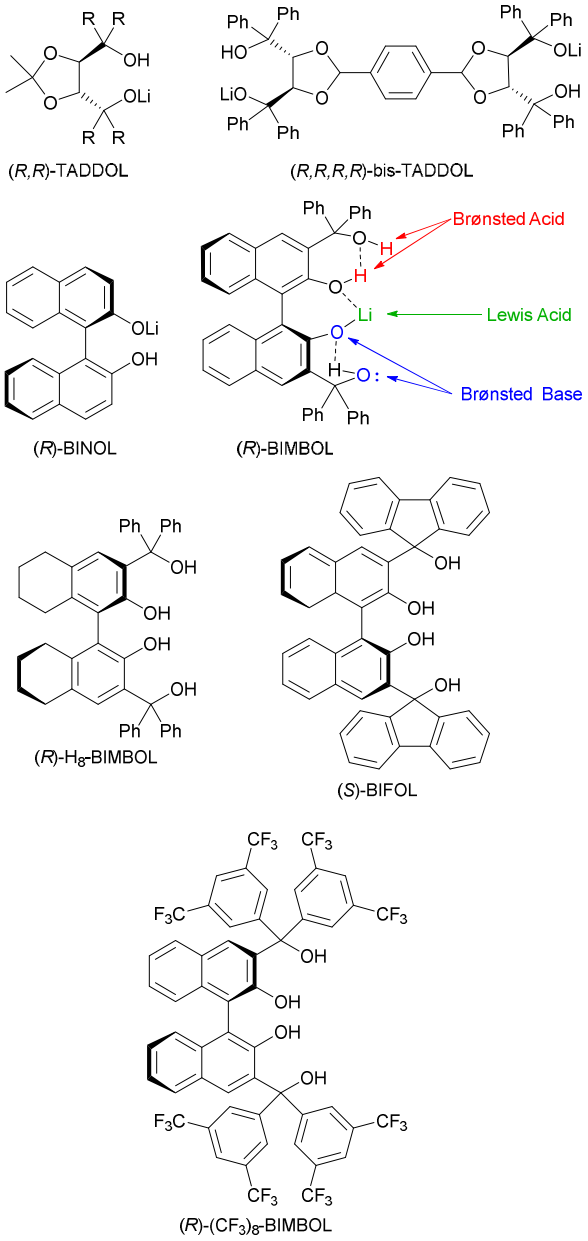

Figure 1: Mono-lithium-salts of chiral polyols: TADDOL, bis-TADDOL, BINOL and BIMBOL and the BINOL derivatives used in this work.

bond forming reactions.[10] The combination of both BINOL and TADDOL motifs in the same molecule to form BIMBOL lithium salt (Figure 1) improved the catalytic performance of the system, compared to the corresponding salts of either BINOL or TADDOL in the benchmark reaction of the Michael addition of diethyl malonate (***MD***) to cyclohexanone (***MA***).[11] The BIMBOL catalyst system has the potential to be trifunctional with the metal ion serving as a Lewis acid whilst the naphtholate ion and hydroxyls are Brønsted base and Brønsted acids respectively.

The enantioselectivity and chemical yields of the BIMBOL catalysed reaction displayed concentration dependences, indicating that the catalyst self-associates to give species with different relative activities.[11] The self-association of lithium derivatives is a well-known phenomenon[12] as is the self-association of derivatives of thiourea,[3i,j,k] catalytically active silanediols[13] and bis-TADDOLs.[10c] This self-association can be an impeding factor for the catalytic activity of amine-thioureas[3i,j] or a favourable one for electrostatically enhanced thioureas,[3k] silanediols[13] and bis-TADDOLs.[10c] Therefore, we have carried out a combined experimental and computational study of the Michael addition of diethyl malonate to cyclohexanone catalysed by lithium salts of BIMBOL and related compounds and show that the reaction exhibits the positive catalytic features associated with enzymatic catalysis.

Results and Discussion

Synthesis of (*R*)- and (*S*)-BIMBOL was achieved as reported earlier.[14] The syntheses of (*R*)-H_8-BIMBOL, (*S*)-BIFOL and (*R*)-$(CF_3)_8$-BIMBOL were achieved from (*R*)- or (*S*)-BINOL (S59†). H_8-BIMBOL should have lower acidity (greater pK_a value) than BIMBOL, whereas $(CF_3)_8$-BIMBOL should be more acidic (lower pK_a value).

The structure of (*R*)-BIMBOL (Figure 2 top) has previously been determined by X-ray crystallography[11] and shown to have two pairs of OH groups each involved in two pairs of intramolecular hydrogen bonds: naphthol-OH···OH-alcohol and vice-versa and with both pairs of OH groups situated over the same face of the naphthyl moieties of BIMBOL (endo-type orientation).[11] X-ray analysis of BIFOL‡ also showed that each pair of OH groups was involved in intramolecular hydrogen bond formation; but the triphenylmethanol groups were positioned on different faces of the naphthyl planes (exo-type orientation, Figure 2 bottom). This raises the question as to whether rotation around the C3-C17 (or C11-C26) bond is hindered to such an extent as to make the exo-isomer observed in the solid state also the atropoisomer present in solution or whether the exo/endo transition is relatively facile in solution. Literature data on the rotation barriers for a series of closely related 2-methyl-1-naphthyl-fluorenes[15] indicated that the energy of rotation around a naphthyl-fluorene bond is >26 kcal/mol. Our calculation of the barrier to rotation in BIFOL from DFT data (S34†) gave a value of 16.6 kcal/mol.

The ^{1}H NMR spectra of BIMBOL and BIFOL in CD_2Cl_2 between 30 °C and −60 °C differed drastically (S55-S56†). While all the resonances of BIFOL (especially those of the OH groups) became narrower as the temperature was lowered, all the resonances of BIMBOL became broader and those of OH groups separated into several sets. Similarly, the ^{13}C NMR spectra of BIFOL and BIMBOL recorded at 30 °C and −40 °C differed immensely (S57-S58†). At 30 °C, the ^{13}C NMR spectrum of BIFOL displayed broad signals for the ipso-carbon atoms bonded to the OH groups (157.7 and 91.7 ppm) and those connecting two binaphthyl moieties (122.7 ppm), whereas the analogous ^{13}C resonances of BIMBOL (156.5, 88.3 and 119.7 ppm, respectively) at the same temperature were narrow. In contrast, at −40 °C, all the BIFOL resonances connected with C-OH moieties and those of the C1 and C9 atoms became narrow

View Article Online
DOI: 10.1039/C6CY01697A

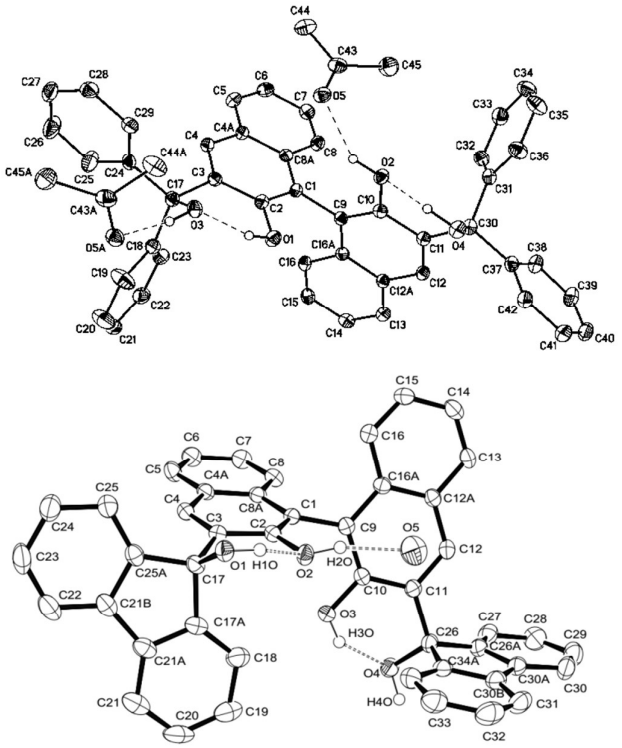

Figure 2: The structures of (*R*)-BIMBOL[11] (top) and (*S*)-BIFOL (bottom) showing the different disposition (endo and exo) of the hydrogen bond coupled OH groups in the crystals of the compounds.

and no change in the number of other resonances took place. However, for BIMBOL at −40 °C, all the resonances became broader and most of them split into multiple signals (S55-S58[†]). Thus, it appears that BIFOL exists in solution at ambient temperature as an interconverting endo-exo-atropoisomer, probably with the isomer depicted in Figure 2 as the major form. Decreasing the temperature slows the OH group proton exchange in BIFOL and as a result, the NMR resonances become progressively narrower and their resolution improves. In contrast, a decrease in temperature in case of BIMBOL caused, in addition to slowing the proton exchange, slow rotation around the sp^3-sp^2 bonds (C17-C3 or/and C11-C30) eventually producing a mixture of several atropoisomeric conformers, existing in a slowly established equilibrium at temperatures below −20 °C.

The benchmark Michael addition of diethyl malonate (***MD***) to cyclohexenone (***MA***) was conducted as shown in Scheme 1. The lithium salt of BIMBOL could be prepared by the reaction of lithium phenoxide with BIMBOL as the pK_a of BINOL in DMSO is approximately 13[16] whereas that of phenol is 18.[17] In addition, it was shown previously that the catalyst generated

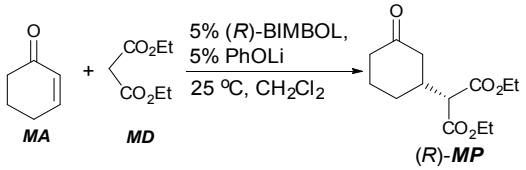

Scheme 1: The addition of diethyl malonate (***MD***) to cyclohexanone (***MA***) using (*R*)-BIMBOL to give (*R*)-***MP***.

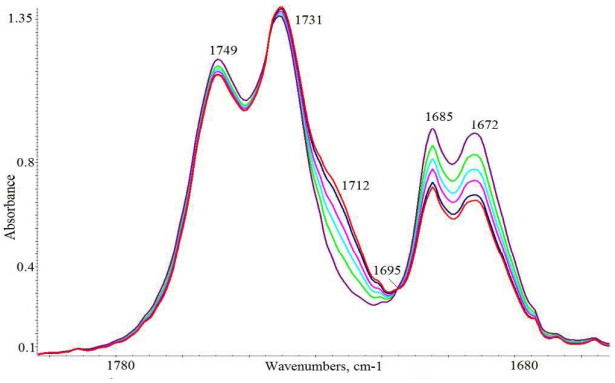

Figure 3: IR monitoring of the ν(CO) region under the reaction conditions: [BIMBOL]=[PhOLi]=0.0057 M, [***MA***]$_o$=[***MD***]$_o$=0.11 M, CH_2Cl_2, 25 °C.

in this manner was catalytically identical to one produced by the reaction of BIMBOL with BuLi.[11]

The reaction could be easily monitored by IR spectroscopy, following the disappearance of the cyclohexenone absorptions at 1671 cm^{-1} (ε = 409) and 1685 cm^{-1} or the appearance of the carbonyl group of the adduct (***MP***) which absorbs at 1712 cm^{-1}. Figure 3 illustrates the progression of the changes of the IR spectra of the reaction mixture under the experimental conditions given in Scheme 1. An isobestic point at 1695 cm^{-1} was observed in the infrared spectra indicating that no side reactions occur during the Michael addition. To allow a quantitative analysis of the kinetic results, curve fitting of the observed spectra in the ν(CO) region was undertaken (see experimental section for details) and the rate of formation of ***MP*** exactly matched the rate of disappearance of ***MA***.

Previously we observed that the reaction took almost 48 hours to go to completion.[11] However, the kinetic data obtained from the infrared spectra and displayed in Figure 4 indicate that the reaction occurs in two kinetically distinct stages (Figure 4, data points a). On the timescale shown in Figure 4, the changes in reactant concentrations are sufficiently small that the data can be fitted to pseudo-zero order kinetics. The rapid, initial section of the reaction produced almost 20% of ***MP*** within 40 minutes. Then, the Michael addition was significantly slowed down. This effect

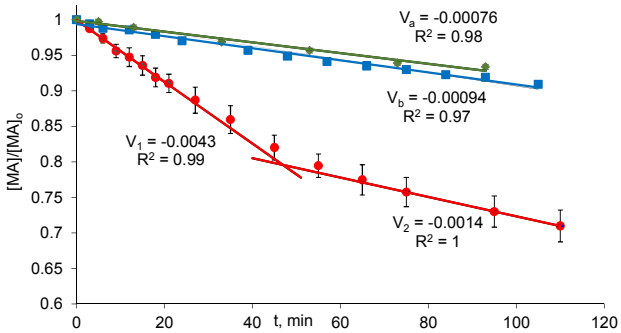

Figure 4: Reaction profile versus time plot for the conversion of cyclohexenone (***MA***) and malonic ester (***MD***) into ***MP*** catalysed by a catalyst prepared in situ from BIMBOL and PhOLi in CH_2Cl_2 under Ar at 25°C: [BIMBOL]=[PhOLi]=0.0057 M, [***MA***]$_o$=[***MD***]$_o$=0.11 M, in CH_2Cl_2; reaction rates (V) are given in min^{-1}. a) no additives b) 10% (relative to ***MA***) of ***MP*** were added. c) half an equivalent of ***MP*** was added.

View Article Online
DOI: 10.1039/C6CY01697A

Table 1: The impact of the ratio of (*S*)-BIMBOL/PhOLi on the reaction kinetics and enantiomeric excess of the resulting ***MP***.[a].

run	(*S*)-BIMBOL, mol%	PhOLi, mol%	V,[b] min^{-1}	*ee* of (*S*)-***MP***,[b]
1	5	5	4.3×10^{-3}	85-90 (86)[c.]
2	5	10	3.0×10^{-3}	86
3	5	2.5	2.8×10^{-4}	78-86
4	10	5	4.6×10^{-4}	83-86

a) The reaction was conducted under Ar at 25 °C, $[\boldsymbol{MA}]_o=[\boldsymbol{MD}]_o=0.11$ M in CH_2Cl_2. b) The initial rate and enantiomeric excess of ***MP*** (the estimated range of three experiments) at 90% conversion. c) The enantiomeric excess of ***MP*** at 15% conversion (the estimated range of three experiments).

$$V = -\frac{[\boldsymbol{MA}]}{dt \cdot [\boldsymbol{MA}]_o} = k \cdot [\boldsymbol{MA}]^x \cdot [\boldsymbol{MD}]^y \cdot [\mathrm{BIMBOL/Li}]^n \quad (1)$$

was assumed to be due to catalyst inhibition by the reaction product and this was supported by the addition of 10–50% of ***MP*** relative to ***MA*** to the reaction mixture. A twofold excess of ***MP*** relative to the catalyst was sufficient to generate a new catalytic species, having lower catalytic efficiency (Figure 4, data points b). A tenfold excess of ***MP*** in the reaction mixture had almost no additional negative effect on the reaction kinetics (Figure 4, data points c).

In order to test if some non-linear effects were present in the system, 10 mol% of ***MP*** with 90% enantiomeric purity was added to the reaction mixture at the beginning of the reaction and the enantiomeric purity of the resulting ***MP*** was checked at 10% and 98% of conversion. In each case the ee of ***MP*** was found to lie in the ee interval of 85-90%. In addition, 10 mol% of racemic ***MP*** was added to the reaction mixture and the final enantiomeric purity of the product was found to be 82% which corresponded to that of a mixture of 10% of a racemic additive and 90% of enantiomerically enriched ***MP*** with ee of 85-90%. Thus, no influence of the ee of ***MP*** on the asymmetric performance of the catalyst was detected.

To determine the order with respect to substrates ***MA*** and ***MD***, reactions were carried out at three concentrations of each substrate whilst keeping the other component concentration constant. The initial zero order rates (up to 15% conversion) of the reactions were determined and the coefficients X and Y in equation 1 were found to be 0.87 and 0.76 respectively. Thus, there was some deviation from the expected second order behaviour, probably, reflecting competition of the substrate present in excess with the other substrate for the active sites of the catalyst.

To address the issue of the real composition of the catalytically active species, reactions were carried out at various ratios of (*S*)-BIMBOL to lithium phenoxide. The malonate carbanion formation should be the key stage of the addition sequence and the amount of basic groups is expected to be the most important feature of the catalyst. Since the number of basic groups in the case of di-Li salts is twice that of mono-Li-salts one could expect doubling the reaction rate. However, the catalytic performance of both was almost the same (Table 1, runs 1 and 2), this indicates that the presence of free hydroxyl groups in the mono-Li salt is an important boost of the catalytic performance of BIMBOL increasing its activity to

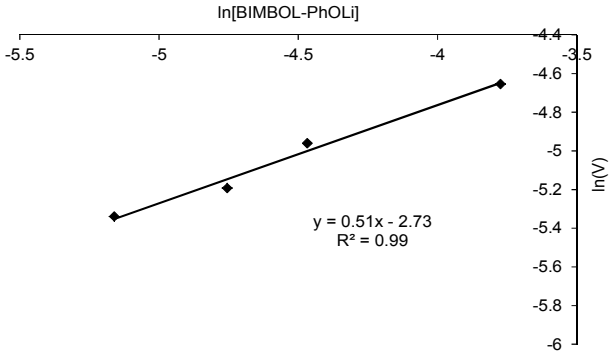

Figure 5: Plot of ln(V) versus ln[Cat] for the addition of diethyl malonate (***MD***) to cyclohexenone (***MA***): (*S*)-BIMBOL/PhOLi 1:1; $[\boldsymbol{MA}]_o=[\boldsymbol{MD}]_o=0.11$ M, solvent CH_2Cl_2.

approaching that of the di-Li salt. However, the ratio of (*S*)-BIMBOL to lithium phenoxide had almost no influence on the enantiomeric excess of the resulting **MP** (Table 1, runs 1-4) which supported the theory that the catalytically active species had the same composition in the reaction mixture whatever the ratio of the catalytic components.

To determine the order with respect to the catalyst concentration, reactions were carried out in duplicate at four different catalyst concentrations. The average initial zero order rate constants (V, min^{-1}) were used to construct a plot of lnV against ln([BIMBOL/Li]). The resulting plot is shown in Figure 5 and the best fit line through the data points has a slope of 0.51±0.16, suggesting that the reaction had a 0.5 order dependence on the catalyst concentration (*n* in equation 1). This indicates that the catalytically active species is monomeric and exists in a rapid equilibrium with a catalytically inert dimeric species, and that the position of equilibrium is strongly shifted towards the dimer (Scheme 2). A very low concentration of the monomeric component in the reaction mixture was supported by the absence of any observable additional signals for either the malonic ester or cyclohexenone protons in their separate 1:1 mixtures with BIMBOL/Li in deuterated dichloromethane solutions (S37†). In contrast, the more acidic ethyl nitropropanoate had its spectrum significantly changed under the same conditions (S37†). The earlier observation of positive non-linear effects in the reaction, with racemic (*S*)- and (*R*)-BIMBOL forming an inert precipitate,[11] provides further indirect evidence for the dimer being catalytically inactive.

In order to investigate the relative importance of Brønsted and Lewis acid centres within the catalyst, lithium complexing agents were added to the reaction mixture and the results are summarised in Table 2. The addition of two equivalents of TMEDA relative to the catalyst completely inhibited the reaction (run 2). The same effect was observed on the addition of just one equivalent of benzo-15-crown-5 (run 3). The addition of three equivalents of THF or morpholine also negatively influenced the yield of the product (runs 4 and 5) although to a lesser extent. On the other hand, three equivalents of 1,2-dimethoxyethane (DME) improved the yield of the product (run 6 and 7) whereas the addition of 20

View Article Online
DOI: 10.1039/C6CY01697A

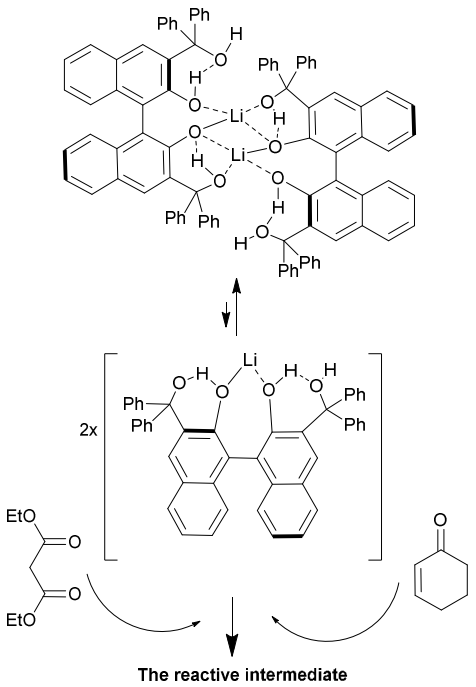

Scheme 2: Illustration of a possible inactive dimer / active monomer equilibrium to rationalise the 0.5 order kinetics relative to the (*S*)-BIMBOL / Li concentration.

Table 2: The influence of coordinating additives on the catalytic performance of (*S*)-BIMBOL / Li.

run	Additive (mol% relative to ***MA***)	Time, h	Yield of (*S*)-***MP***, %[a] (*ee*%)[b]
1	-	48	55 (85-90)
2	TMEDA (10%)	24	0
3	Benzo-15-crown-5 (5%)	24	0
4	THF (15%)	24	22 (n.d.)
5	Morpholine (15%)	24	10 (n.d.)
6	DME (15%)	24	60 (85-90)
7	DME (15%)	48	98 (85-90)
8	DME (100%)	24	0

The reaction was conducted under Ar at 25 °C in CH_2Cl_2, [(*S*)-BIMBOL]=[PhOLi]=0.0124 M, $[\mathbf{MA}]_o=[\mathbf{MD}]_o$=0.248 M. a) The yield was estimated by ^{1}H NMR. b) The enantiomeric excess of the product was determined by chiral HPLC analysis of ***MP***.

Table 3: DOSY experiments[a].

run	Compound	Log D	D x10^9 m^{2}s^{-1}
1	BIMBOL	-9.083	0.808
2	BIMBOL + PhOLi	-9.21	0.61
3	BIMBOL / Li + benzo-15-crown-5 (1:1 relative to Li)	BIMBOL -9.0855 Crown -9.0042	0.821 0.990
4	benzo-15-crown-5	-8.88	1.32
5	BIMBOL / Li / DME (3:1 relative to Li)	-9.18 (BIMBOL) -8.63 (DME)	0.64 2.34
6	DME	-8.52	3.07

a) DOSY experiments were carried out at 20 °C in CD_2Cl_2, [Polyol]=[PhOLi]=0.03 M. The reaction conditions were the same as those given in the footnote to Table 2.

equivalents of DME resulted in complete inhibition of the reaction.

According to DOSY data, summarised in Table 3, the formation of mono lithium salts of BIMBOL led to a reduction of its diffusion coefficient (D) relative to that of BIMBOL from $0.88x10^{-9}$ to $0.61x10^{-9}$ m^{2}s^{-1} (entries 1 and 2). The formation of a dimer of the Li-salt is a reasonable explanation of these results. The addition of benzo-15-crown-5 to BIMBOL / Li in a 1:1 ratio led to an increase of D in the case of the BIMBOL / Li salt (entry 3, D=$0.82x10^{-9}$) and decreased D for the crown ether (entries 3 and 4, D =$0.990x10^{-9}$ m^{2}s^{-1} and $1.32x10^{-9}$ m^{2}s^{-1} respectively). This can be explained by the establishment of a rapid equilibrium between species including significant amounts of monomeric BIMBOL-Li-benzo-15-crown-5. The effect of DME on the BIMBOL-Li was different. The addition of three equivalents of DME had almost no influence on the D of the lithium salt (runs 2 and 5), but the diffusion coefficient of DME itself somewhat decreased (run 5 and 6). This suggests that the interactions of DME were mostly with the lithium monomer present in small amounts in the solution (Scheme 5).

These data show that the lithium cation constituted the core of the catalytic system and its coordination with strong external complexing agents led to the complete loss of the catalytic activity. However, some weakly coordinating agents such as DME could increase the catalytic activity in terms of both yield and enantioselectivity which might indicate a beneficial influence of the additive by thwarting the inhibiting effects of the product ***MP*** on the reaction kinetics and/or shifting the equilibrium of Scheme 5 towards the monomer components.

In order to investigate the relative importance of the BIMBOLate hydroxyl groups in the catalysis, the relative activities of the mono-lithium salts of BIMBOL, BINOL, H_8-BIMBOL, BIFOL, and $(CF_3)_8$-BIMBOL were studied in the model reaction (Scheme 1) under identical conditions and the results are shown in Figure 6 where the initial consumptions of ***MA*** are plotted versus time. As can be seen from Figure 6, BINOL was much less active than BIMBOL. The superior activity of the later was not a consequence of the greater acidity of its phenolic hydroxyl groups, relative to those of BINOL, as the more acidic $(CF_3)_8$-BIMBOL also displayed a diminished activity relative to BIMBOL.

H_8BIMBOL-Li had a different type of reactivity with an induction period observed at the beginning of the reaction, followed by a lower reaction rate than that of BIMBOL-Li. The induction period may reflect slow dissociation of the dimeric lithium salt, initiated by the substrates. Such processes were shown to become rate limiting in some reactions of lithium derivatives.[12b] (*R*)-H_8-BIMBOL led to ***MP*** of (*R*)-configuration, as also observed for (*R*)-BIMBOL (see Table 1), though with a diminished enantiomeric excess of 25% after 1.5 h and 26% after 27 h. In addition, at longer time intervals, the rate of the H_8BIMBOL-Li promoted reaction became faster than that of the BIMBOL-Li catalysed one. It took only 24 h for H_8-BIMBOL-Li to bring the reaction to 80% completion, whereas BIMBOL-Li furnished only 55% of ***MP*** within that time interval. The difference in behaviour of BIMBOL and H_8BIMBOL can be due

DOI: 10.1039/C6CY01697A

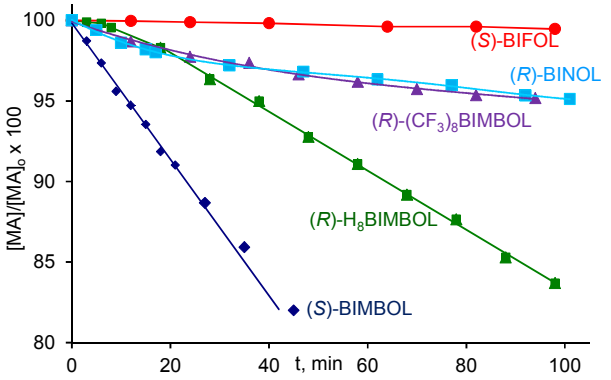

Figure 6: Relative activities of the mono-lithium salts of (*S*)-BIMBOL, (*R*)-BINOL, (*R*)-H_8BIMBOL, (*S*)-BIFOL, and (*R*)-$(CF_3)_8$BIMBOL in the model Michael addition reaction in CH_2Cl_2 at 25°C: [tetraol]=[PhOLi]=0.0057 M, [***MA***]$_o$ [***MD***]$_o$=0.11 M.

to the variation in their acidity and in the torsion angles of their naphthyl moieties. The acidities of BINOL and H_8BINOL in DMSO are 13.2 and 17.9 respectively[17] and the minimum energy torsion angle is greater in case of H_8-BINOL than for BINOL. The same trend could be expected to be retained in BIMBOL, and H_8-BIMBOL with the torsional angle in the latter being greater by approximately six degrees, making the OH groups of the naphthyl moieties closer to each other (according to MM2 calculations). These two factors combined could produce the observed effects. One of the reasons for the greater activity of H_8BIMBOL-Li at the later stages of the reaction could be the less likely formation of the non-productive complex with ***MP*** because of the combined acidity/steric properties of H_8-BIMBOL-Li.

(*S*)-BIFOL was even less active than BINOL (Figure 6) and even after 48 hours no ***MP*** formation was observed under the standard conditions with BIFOL-Li catalyst. Several explanations could be put forward to rationalise the lack of catalytic activity of BIFOL-Li:

1. The four OH group are unable to form hydrogen bond supported trimolecular ***MA*** and ***MD***$^{-1}$ (deprotonated ***MD***) complexes with BIFOL in which the Michael acceptor and donor are situated in appropriate positions for carbon–carbon bond formation to take place, as hypothesised previously.[11]

2. The observation could be connected to the slow rotation of the hydroxyfluorenyl moieties around the sp^2–sp^3 bonds C(17)-C(3) or C(11)-C(26) (S34†). The release of ***MP*** from the catalytic site of the BIMBOLs and, thus, recovery of the catalyst should be coupled to the breaking of hydrogen bonds between the carbonyl groups of ***MP*** and the OH groups of BIMBOLs. This might necessarily involve the conformational rearrangement of the endo- to exo-orientation of the triphenylcarbinol moieties of BIMBOLs. In the case of BIFOL such conformational rearrangement is too slow (*vide supra*) and results in very slow catalyst release and slowing of the reaction.

3. Another explanation might be based on a slow Li-dimer–monomer dissociation in the case of BIFOL also linked to the slow conformational rearrangements.

Thus, the presence of four interconnected OH groups with endo-orientation inside the same chiral molecule is a prerequisite for the efficient performance of the catalyst family. The variation in their acidities, mutual orientation and the rate of the conformational rearrangements could be decisive factors in determining the catalyst activity of the system. Finally, the presence of a Lewis acidic lithium counter-cation is a prerequisite for efficient BIMBOL-Li catalysis.

In order to shed light on the details of the reaction mechanism, DFT calculations were performed on the system. For analysis of the intramolecular interactions QTAIM theory[18] was used as that gives an opportunity to locate all the bonding interactions by a critical point search as well as to estimate the energy of the interactions by means of Espinosa correlation.[19] Firstly, optimisation for two overall uncharged complexes **Li1** and **Li2** were carried out. The first complex **Li1** contained the anion of BIMBOL, one lithium cation and a neutral malonic ester (Figure 7, top) whereas **Li2** contained a neutral BIMBOL, one lithium cation and a malonic ester anion (Figure 7, bottom). In both complexes, the lithium cation is tetracoodinated by two oxygen atoms of BIMBOL and two oxygen atoms of the carbonyl groups of malonic ester. At the same time in **Li1** the lithium cation is coordinated by oxygen atoms of the same naphthalene fragment (O(1) and O(2)) whereas in **Li2** it forms bonds with both fragments (O(1) and O(3) atoms). As expected, in the **Li1** complex, the Li-O distance with deprotonated O(2) atom is the shortest (1.852 Å), while the corresponding bonds with OH groups vary in the range of 1.892-1.917 Å. In contrast, the Li-O bonds with carboxy groups of malonic ester are shorter in the case of **Li2**. The additional stabilisation of the **Li1** and **Li2** salts is also due to O(3)-H···O(4), O(4)-H···O(7) and O(3)-H···O(4) hydrogen bonds respectively. Furthermore, the number of HO…OH and O(4)-H···C(2) interactions in **Li2** have been established by a critical point search. The latter interactions can be interpreted as the O-H···OH hydrogen bonds and can serve as the channel of proton transfer from the BIMBOL molecule to the malonic ester anion and, according to the principle of microscopic reversibility, the chain of proton removal from the neutral malonic ester to the ionised BIMBOL. The energy of these C-H···O and O-H···O interactions are 2.0 and 3.2 kcal/mol respectively. Despite the significant difference in charge distribution and intramolecular interactions in **Li1** and **Li2** their total energy was almost equal, with **Li2** being just 2.0 kcal/mol lower in energy.

Generally**,** **Li1** and **Li2** differ mostly in the position of a proton on either BIMBOL or malonic ester moieties within their complexes. In other words, the two structures represent the limiting extremes of an acid-base equilibrium, involving BIMBOL-phenolate/BIMBOL conjugated acid and malonic-ester/malonate-anion. Taking into account that the acidities of BINOL and malonic esters in DMSO are 13.2[17] and 16.4,[18] respectively; such a small difference in energy between **Li1** and **Li2** was unexpected. It could be an indication of a greatly increased acidity of the coordinated malonic ester by the stabilisation of malonate anion in **Li2**, as compared with the free CH-acid. Such stabilisation may originate from the lithium cation coordination of the malonate and also from the

View Article Online
DOI: 10.1039/C6CY01697A

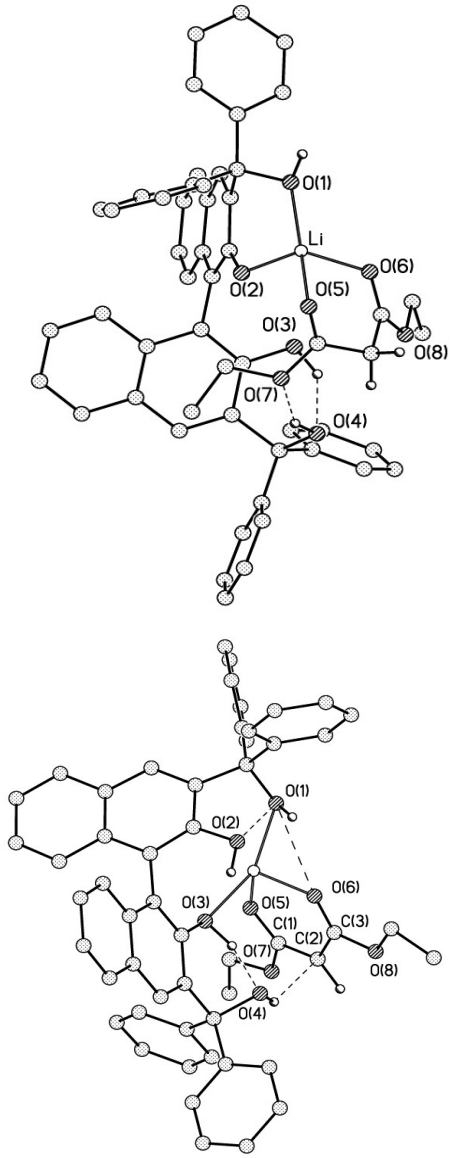

Figure 7: Views of **Li1** (top) and **Li2** (bottom) according to DFT calculations. Some hydrogen atoms are omitted for clarity. The intramolecular interactions are shown only for contacts for which the critical points (3,-1) of the electron density function were located.

O(4)-H···C(2) hydrogen bond, linking the BIMBOL moiety and malonate.

As the next step, energy calculations on the ***MA*** adducts with both **Li1** and **Li2** (**Li1MA**, **Li2MA** and **Li3MA**) were conducted. In contrast to **Li1** and **Li2,** the total energies of complexes **Li1MA**, **Li2MA** and **Li3MA** (Figure 8) differed significantly, with the additional stabilisation of the latter two adducts by 13.6 and 13.5 kcal/mol respectively. The energies of interaction of ***MA*** with **Li1** and **Li2** were calculated to be 11.0 and 22.6 kcal/mol in **Li1MA** and **Li2MA** respectively. An alternative conformation of ***MA*** with **L1** was also considered (S17[†]). In both complexes, the main force that binds ***MA*** is a O(1)-H···O(9)=C bond with an energy of 10.4 and 11.6 kcal/mol respectively. In addition to this hydrogen-bond, in **Li2MA** there

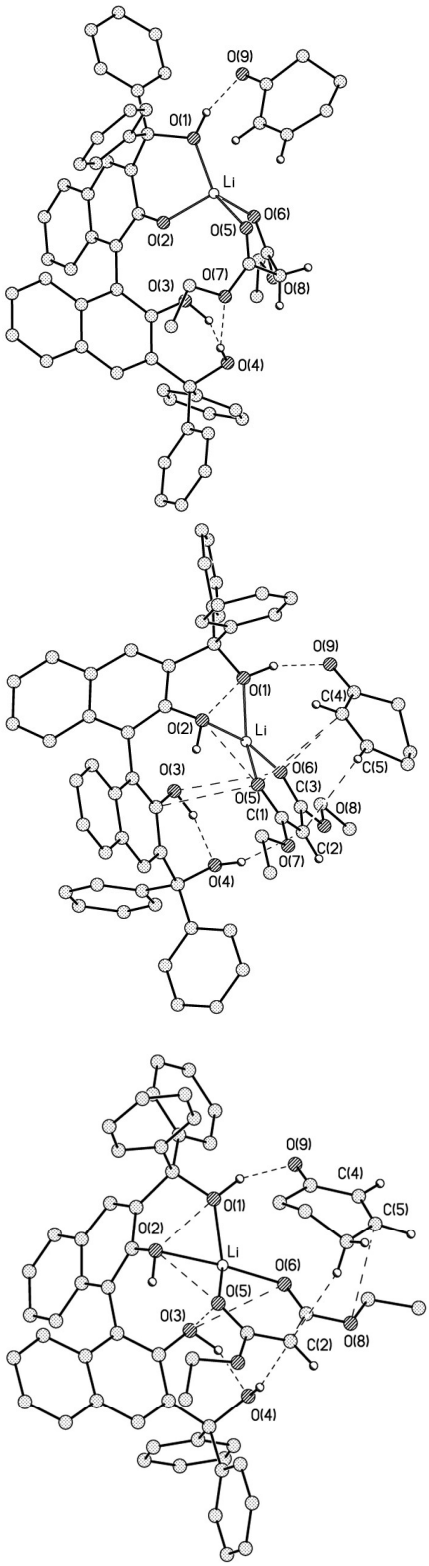

Figure 8: Views of **Li1MA** (top), **Li2MA** (middle) and **Li3MA** (bottom) according to the results of DFT calculations. Some hydrogen atoms are omitted for clarity. Intramolecular interactions are shown only for contacts for which critical points (3,-1) of electron density function were located.

View Article Online
DOI: 10.1039/C6CY01697A

are a number of additional interactions such as C···C (3.58 Å) and O···C (3.2-3.3 Å) between the malonate anion and ***MA*** with energy varying in the range of 0.7-1.2 kcal/mol.

The **Li3MA** structure differed from **Li2MA** by rotation of the ***MA*** moiety by 180 degrees around the O(1)H···O(9)=C bond (Figure 8). Although the energy of this complex was almost equal to that of **Li2MA** (it is less stable by only 0.12 kcal/mol), the type and number of interatomic interactions between the cyclohexenone and malonate were different. In contrast to the C(2)···(C5); O(5)···C(4) and O(6)···C(4) interactions in **Li2MA,** the atoms of the C=C bond of ***MA*** in **Li3MA** interact only with the O(8) atom (O···C 3.68 Å) and with the C(2) atom of the malonate by one of the ***MA*** aliphatic protons. The distances between C(2) and C(5) are 3.58 Å in L**i2MA** and 4.2-4.28 Å in **Li3MA**. All other interactions in **Li3MA** are similar to those in **Li2MA.**

Thus, according to the DFT calculations, the ionisation of ***MD*** occurs by its α-proton being removed by the alcohol oxygen atom O(4) of BIMBOL-Li facilitated by proton distribution via the chain of hydrogen bonds inside **Li1**, leading to formation of **Li2** existing in a facile equilibrium with **Li1**. However, the formation of the reactive intermediates BIMBOL^{0}-Li^{+1}-x***MA***-x***MD***$^{-1}$ (**Li2MA** and **Li3MA,** Figure 8) occurs by the addition of ***MA*** to **Li2** and not **Li1**. Within adducts **Li2MA** and **Li3MA** the electrophilicity of the molecule of ***MA*** is greatly increased by the O(1)-H···O(9) hydrogen bond formation with the BIMBOL moiety. The mutual disposition of both ***MA*** and ***MD*** inside the intermediate complex **Li2MA** or **Li3MA** is ideal for the final carbon-carbon bond formation. The generation of ***MP*** can be easily portrayed as proceeding by the formation of a carbon-carbon bond between C(2) of ***MD***$^{-1}$ and C(5) of ***MA*****.** The negative charge transfer is most likely being accompanied by a chain of proton transfers[20] from O(1)-H to O(9) and from O(2)-H to O(1). Thus, there are no significant changes in the position of atoms and charges in the transition state of the carbon-carbon bond formation leading to ***MP***.

It is the (*R*)-**Li3MA** intermediate that should lead to the expected *R*-configuration of ***MP*** (Table 1 and 2) whereas (*R*)-**Li2MA** should give rise to ***MP*** with *S*-configuration. As the energy of both intermediates are almost equal, it is the energies of the relative transition states and not the initial intermediates that determine the stereochemical outcome of the carbon-carbon bond formation.

Conclusions

The family of tetraols, studied in this work, provide an interesting catalytic behaviour reminiscent of enzymatic catalysis. Features such as positioning of two substrates on the same catalytic centre, product inhibition of the catalysis and proton transfer through a chain of hydrogen bonds can all be found in typical enzymatic reactions. In addition, the trifunctional catalyst derived from BIMBOL-Li displays a sophisticated behaviour with its capabilities concealed by the intrinsic self-association phenomena. The BIMBOL scaffold should be a versatile unit for the generation of asymmetric catalysts and the mechanistic work reported herein not only allows a better understanding of this Michael addition, but will facilitate the design and development of other highly effective asymmetric catalysts based on BIMBOL and related polyol catalysts. Work in this direction is continuing in our group.

Experimental

General experimental, crystallographic and computational details are given in the supporting information.

(*R*)-BIMBOL. Synthesised by the previously reported method[21] starting from (*R*)-BINOL. $[\alpha]_D^{25}$ +109.8 (*c* 1.00, $CHCl_3$), lit.[21] $[\alpha]_D^{20}$ +113.4 (*c* 1.00, $CHCl_3$); Mp. 186–188 °C, (lit.[22] mp. 176–179 °C); ^{1}H NMR (300 MHz, $CDCl_3$) δ 7.68–7.65 (m, 2H), 7.40–7.28 (m, 24H), 7.19 (s, 2H), 7.17–7.14 (m, 2H), 6.70 (s, 2H), 4.79 (s, 2H); Found (%): C, 79.2; H, 5.8. $C_{46}H_{34}O_4 \times 2H_2O \times (CH_3)_2CO$. Calculated (%): C, 78.9; H, 5.9.

***(R)*-H_8-BINOL.** (*R*)-BINOL (5 g, 17.5 mmol), Pd/C 10% wt (1.5 g), EtOH (39 ml) and H_2O (1 ml) were charged into a 200 ml steel autoclave. The reaction was carried out at a pressure of 70 atm. of H_2 and 120 °C for 5 hours. The product was purified by flash chromatography on SiO_2 (*n*-hexane/EtOAc 5:1). Recrystallisation from *n*-hexane gave (*R*)-H_8-BINOL (3.8 g, 76%) as a white powder. Measured: $[\alpha]_D^{25}$ +51.8 (*c* 2.00, $CHCl_3$); mp. 149-151 °C; ^{1}H NMR (400 MHz, $CDCl_3$) δ 7.10 (d, *J* = 8.3 Hz, 2H), 6.85 (d, *J* = 8.3 Hz, 2H), 4.59 (s, 2H), 2.77 (t, *J* = 6.2 Hz, 4H), 2.40–2.08 (m, 4H), 1.87–1.64 (m, 8H). Literature data[23] for (*S*)-enantiomer: $[\alpha]_D^{20}$ −49.3 (*c* 1.00, $CHCl_3$), mp. 156–157 °C.

***(R)*-MOM-H_8-BINOL.** To a suspension of 55% NaH (1.2 g, 34.3 mmol) in THF (80 ml) under argon at 0 °C was added a solution of (*R*)-H_8-BINOL (3.8 g, 13.3 mmol) in THF (18 ml). The reaction mixture was stirred at this temperature for 1 hour, then MOMCl (4.0 ml, 46 mmol) was added and the reaction left overnight. H_2O (50 ml) was added to the reaction mixture which was then extracted with CH_2Cl_2 and washed with brine. The organic layer was dried over $MgSO_4$, the solvent removed in vacuo and the residue was recrystallised from *n*-hexane to give (*R*)-MOM-H_8-BINOL (4.66 g, 92%) as a white solid. Measured $[\alpha]_D^{25}$ +47.8 (*c* 2.00, $CHCl_3$); ^{1}H NMR (300 MHz, $CDCl_3$) δ 7.07 (d, *J* = 8.5 Hz, 2H), 6.97(d, 2H, *J*=8.5 Hz), 5.03 (d, *J* =6.7 Hz, 2H) 4.98 (dd, *J* =6.7 Hz, 2H), 3.36 (s, 6H), 2.44–2.13 (m, 4H), 1.89–1.63 (m, 8H). Literature data for (*S*)-enantiomer[24] $[\alpha]_D^{25}$ −46.6; ^{1}H NMR corresponded to the lit. data.[26]

(*R*)-MOM-H_8-BIMBOL. To a solution of (*R*)-MOM-H_8-BINOL (1.4 g, 3.6 mmol) in dry distilled THF (55 ml) under argon at −5 °C, a 2.5 M hexane solution of nBuLi (5.8 mL 14.6 mmol) was added dropwise with stirring. The reaction mixture was stirred at this temperature for 3 hours, then benzophenone (2.0 g, 11.0 mmol) was added and the reaction left stirring overnight at room temperature. The reaction was then neutralised by the addition of 0.1 M aqueous HCl. THF was removed in vacuo, the residue was extracted with CH_2Cl_2, the organic layer washed with water and then dried over $MgSO_4$. The solvent was removed in vacuo. The product was recrystallised from MeOH

View Article Online
DOI: 10.1039/C6CY01697A

to give white crystals of (*R*)-MOM-H_8-BIMBOL (1.2 g, 45%). $[\alpha]_D^{25}$ +11.5 (c 1.00, $CHCl_3$); mp. 222–224 °C; ^{1}H NMR (400 MHz, $CDCl_3$) δ 7.47–7.22 (m, 20H), 6.36 (s, 2H), 5.92 (s, 2H), 4.01 (d, *J* =4.6 Hz, 2H), 3.96 (d, *J* =4.6 Hz, 2H), 2.97 (s, 6H), 2.68–2.49 (m, 4H), 2.44–2.19 (m, 4H), 1.79–1.63 (m, 8H); ^{13}C NMR (101 MHz, $CDCl_3$) δ 150.51, 147.23, 146.95, 138.61, 136.97, 132.70, 131.54, 130.82, 127.94, 127.74, 127.72, 127.10, 97.55, 81.81, 56.88, 29.61, 27.72, 22.90 (2C).

(*R*)-H_8-BIMBOL. To a solution of (*R*)-MOM-H_8-BIMBOL (1.2 g, 16.0 mmol) in THF (24 ml) was added 3N aqueous HCl (4.7 ml) and the reaction heated under reflux for 5 hours. After cooling to room temperature, the reaction mixture was neutralized with 5% aqueous Na_2CO_3. Then it was extracted with CH_2Cl_2, dried over $MgSO_4$, the solvent was removed in vacuo and the resulting solid purified by silica gel column chromatography (eluent: *n*-hexane/EtOAc 3:1) to give (*R*)-H_8-BIMBOL (0.42 g, 40%) as a white solid. $[\alpha]_D^{25}$ +50 (c 0.5, $CHCl_3$); mp. 116 °C (decomp.); ^{1}H NMR (400 MHz, $CDCl_3$) δ 7.42–7.16 (m, 20H), 6.26 (s, 2H), 5.99 (s, 2H), 4.60 (s, 2H), 2.58–2.50 (m, 4H), 2.32–2.12 (m, 4H), 1.79–1.61 (m, 8H); ^{13}C NMR (101 MHz, $CDCl_3$) δ 149.59, 146.21, 145.72, 136.98, 130.90, 129.74, 128.89, 127.93, 127.88, 127.79, 127.73, 127.31, 121.25, 82.64, 77.33, 29.38, 26.95, 22.98, 22.92; Found (%): C, 83.3; H, 6.6. Calculated for $C_{46}H_{42}O_4$ (%): C, 83.9; H, 6.4.

(*S*)-MOM-BINOL. The preparation of (*S*)-MOM-BINOL was carried out by the same method used for (*R*)-MOM-H_8-BINOL and gave (*S*)-MOM-BINOL as a white solid, in 90% yield, m.p. 101-102 °C. ^{1}H NMR (400 MHz, $CDCl_3$) δ 7.97 (d, *J* =9.0 Hz, 2H), 7.90 (d, *J* =8.0 Hz, 2H), 7.50–7.33 (m, 4H), 7.27–7.23 (m, 2H), 7.18 (d, *J* = 8.3 Hz, 2H), 5.17 (d, *J* =6.24 Hz, 2H), 4.9 (d, *J* =6.2 Hz, 2H), 3.19 (s, 6H). Literature data m.p. 102-103 °C.[25]

(*S*)-BIFOL. To a solution of (*S*)-MOM-BINOL (2.0 g, 5.4 mmol) in dry distilled THF (50 ml) under argon at −5 °C, a 2.5 M hexane solution of nBuLi (7.5 mL, 18.7 mmol) was added dropwise with stirring. The reaction mixture was stirred at this temperature for 3 hours, then 9H-fluoren-9-one (2.4 g, 13.3 mmol) was added and the reaction left stirring overnight at room temperature. The reaction was quenched by the addition of saturated aqueous NH_4Cl. THF was removed in vacuo, the residue extracted with CH_2Cl_2 and washed with water. The organic layer was dried over $MgSO_4$, the solvent removed in vacuo to give (*S*)-MOM-BIFOL which was deprotected without further purification. The (*S*)-MOM-BIFOL was dissolved in dimethoxyethane (100 ml) and 6N aqueous HCl (64 ml) added. The reaction was stirred at room temperature for 3 days, then neutralised with 5% aqueous Na_2CO_3, extracted with CH_2Cl_2 and dried over Na_2SO_4. The solvent was removed in vacuo and the product purified by silica gel column chromatography (eluting with petroleum ether/EtOAc 5:1, then 2:1). The resulting material was dried under vacuo over P_2O_5 and paraffin at the temperature of boiling toluene to give (*S*)-BIFOL (1.64 g, 47%) as a pale yellow crystalline compound. $[\alpha]_D^{25}$ +52.4 (c 0.21, $CHCl_3$); mp. 200 °C (decomp.); ^{1}H NMR (400 MHz, $CDCl_3$) δ 9.37 (br s, 2H), 8.07 (d, *J* = 7.1 Hz, 2H), 7.96 (dd, *J* = 20.3, 9.1 Hz, 4H), 7.92–7.82 (m, 4H), 7.69 (dd, *J* = 14.5, 7.2 Hz, 6H), 7.62–7.41 (m, 10H), 4.62 (br s, 2H); ^{13}C NMR (101 MHz, $CDCl_3$) δ 152.26, 149.24, 148.44, 139.75, 139.32, 133.92, 129.66, 129.60, 129.42, 128.82, 128.72, 128.51, 128.42, 126.88, 126.82, 125.34, 124.94, 124.71, 123.70, 120.37, 120.32, 116.88, 86.38; Found (%): C, 85.3; H, 4.2. Calculated for $C_{46}H_{30}O_4$ (%): C, 85.4; H, 4.7.

(*R*)-MOM-BINOL. The preparation of (*R*)-MOM-BINOL was carried out by the same method used for (*R*)-MOM-H_8-BINOL and gave (*R*)-MOM-BINOL as a white solid in 91% yield.

(*R*)-Diethyl-MOM-BICBOL. To a solution of (*R*)-MOM-BINOL (2.8 g, 7.5 mmol) in dry distilled THF (110 ml) under argon at −5 °C, a 2.5 M hexane solution of nBuLi (12.7 ml, 31.8 mmol) was added dropwise with stirring. The reaction mixture was stirred at this temperature for 3 hours, then the resulting suspension was added dropwise to diethyl carbonate (70 ml) at 0 °C and left to stir overnight at room temperature. The reaction was then neutralised by addition of 0.1 M aqueous HCl. THF was removed in vacuo, the residue extracted with CH_2Cl_2 and washed with water. The organic layer was dried over $MgSO_4$ and the solvent was removed in vacuo. The residue was purified by silica gel column chromatography (eluent: petroleum ether/EtOAc 4:1) to give (*R*)-diethyl-MOM-BICBOL (1.2 g, 31%) as a white solid. $[\alpha]_D^{25}$ +80.9 (c= 1, $CHCl_3$); ^{1}H NMR (400 MHz, $CDCl_3$) δ 8.56 (s, 2H), 7.98 (d, *J* = 8.1 Hz, 2H), 7.48 (t, *J* = 7.5 Hz, 2H), 7.37 (m, 2H), 7.30 (d, *J* = 8.5 Hz, 2H), 4.86 (m, 4H), 4.47 (q, *J* = 7.1 Hz, 4H), 2.50 (s, 6H), 1.46 (t, *J* = 7.1 Hz, 6H). Literature data for (*R*)-enantiomer[26] $[\alpha]_D^{20}$ +87.7 (c =0.24, $CHCl_3$). ^{1}H NMR corresponded to the lit data.[28]

(*R*)-MOM-$(CF_3)_8$-BIMBOL. To a solution of (*R*)-diethyl-MOM-BICBOL (1.2 g, 2.3 mmol) in THF (22 ml) under an argon atmosphere at 0 °C, a 0.5 M THF solution of 3,5-di(trifluoromethyl)phenylmagnesium bromide (25 ml, 12.5 mmol) was added, then the reaction was left overnight at room temperature. The reaction was quenched with saturated aqueous NH_4Cl, extracted with CH_2Cl_2 and washed with water. The organic layer was dried over $MgSO_4$ and solvent was removed in vacuo. The residue was purified by silica gel column chromatography (eluent: hexane, then hexane/EtOAc 5:1) to give (*R*)-MOM-$(CF_3)_8$-BIMBOL (2.6 g, 88%) as a mixture of conformers. Data for the major conformer: ^{1}H NMR (300 MHz, $CDCl_3$) δ 8.82–7.95 (m, 12H), 7.71 (d, *J* = 8.2 Hz, 2H), 7.50–7.38 (m, 4H), 7.18 (d, *J* = 8.3 Hz, 2H), 7.05 (s, 2H), 6.45 (s, 2H), 4.37 (d, *J* = 5.9 Hz, 2H), 4.01 (d, *J* = 5.9 Hz, 2H), 3.03 (s, 6H); ^{19}F NMR (376 MHz, $CDCl_3$) δ 14.94 (s), 14.70 (s); ^{13}C NMR (101 MHz, $CDCl_3$) δ 153.00 (s), 149.49 (s), 147.05 (s), 137.27 (s), 134.20 (s), 132.45–130.91 (m), 131.20 (s), 129.63 (s), 129.21 (s), 128.68 (s), 127.94 (s), 127.26 (d, *J* = 7.1 Hz), 126.43 (s), 125.64 (s), 125.17 (s), 124.54 (d, *J* = 7.2 Hz), 121.51–122.10 (m), 119.12 (d, *J* = 7.0 Hz), 99.73 (s), 80.01 (s), 57.53 (s); Found (%): C, 54.1; H, 2.7; F, 35.4. Calculated for $C_{58}H_{34}O_6F_{24}$ (%): C, 54.3; H, 2.7; F, 35.5.

View Article Online
DOI: 10.1039/C6CY01697A

(*R*)-(CF$_3$)$_8$-BIMBOL. To a solution of (*R*)-MOM-(CF$_3$)$_8$-BIMBOL (2.6 g, 2.0 mmol) in dioxane (65 ml), 26% aqueous HCl (28 ml) was added and the reaction heated under reflux at 60 °C for 7 hours. The reaction mixture was quenched with aqueous Na_2CO_3 until it was just slightly acidic, extracted with CH_2Cl_2, washed with water, dried over $MgSO_4$ and solvent was removed in vacuo. The residue was purified by silica gel column chromatography (hexane then hexane/acetone 1:1) to give (*R*)-(CF$_3$)$_8$-BIMBOL (1.5 g, 63%) as a beige crystalline solid. $[\alpha]_D^{25}$ −96.8 (c 1.00, $CHCl_3$); mp. 175 °C; ^{1}H NMR (400 MHz, $CDCl_3$) δ 7.94 (d, *J* = 20.3 Hz, 4H), 7.85 (d, *J* = 8.4 Hz, 8H), 7.76 (d, *J* = 7.2 Hz, 2H), 7.53–7.39 (m, 4H), 7.14–7.07 (m, 4H), 5.60 (s, 2H), 5.20 (s, 2H); ^{19}F NMR (376 MHz, $CDCl_3$) δ 14.93 (s), 14.85 (s). ^{13}C NMR (101 MHz, $CDCl_3$) δ 149.65 (s), 147.74 (s), 146.32 (s), 132.81 (s), 132.44 (s), 132.10 (s), 131.77 (s), 131.73 (s), 131.36 (s), 129.51 (s), 129.35 (s), 128.51 (s), 127.76 (br s), 127.21 (br s), 125.91 (s), 124.45 (s), 123.19 (s), 122.32 (br s), 121.74 (s), 112.76 (s), 80.89 (s); Found (%): C, 53.9; H, 2.5; F, 37.8. Calculated for $C_{54}H_{26}O_4F_{24}$ (%): C, 54.3; H, 2.2; F, 38.2.

Diethyl (*S*)-2-(3-oxocyclohexyl)malonate (*MP*). To a solution of (*S*)-BIMBOL (8.1 mg, 0.0124 mmol), PhOLi (1.3 mg, 0.013 mmol) and cyclohexenone (23.8 mg, 0.248 mmol) in anhydrous CH_2Cl_2 (1 ml) under argon at room temperature diethyl malonate (39.7 mg, 0.248 mmol) was added and the reaction was stirred for 48 hours. Then the reaction was quenched by adding acetic acid, the mixture was evaporated and diethyl (*S*)-2-(3-oxocyclohexyl)malonate isolated as a colourless oil (60.0 mg, 94%) by preparative thin layer chromatography eluting with petroleum/EtOAc 5:1. $[\alpha]_D^{25}$ −2.7 (c 0.5, $CHCl_3$); ^{1}H NM R (400 MHz, $CDCl_3$) δ 4.22 (qd, *J* = 7.1, 4.1 Hz, 4H), 3.31 (d, *J* = 7.9 Hz, 1H), 2.55 (dtd, *J* = 15.2, 7.8, 3.7 Hz, 1H), 2.44 (t, *J* = 17.0 Hz, 2H), 2.36–2.20 (m, 2H), 2.14–2.04 (m, 1H), 1.98 (d, *J* = 12.7 Hz, 1H), 1.81–1.61 (m, 1H), 1.62–1.45 (m, 1H), 1.29-1,20 (m, 6H), Found (%): C, 61.4; H, 7.8. Calculated for $C_{13}H_{20}O_5$ (%): C, 60.9; H, 7.9. $[\alpha]_D^{25}$ -2.7 (c 1.00, $CHCl_3$) Enantiomeric analysis: CHIRALPAK AS-H column (4.6 mm i.d. x 250 mm); eluent n-hexane/2-propanol = 90:10; flow rate 1.0 ml/min; detection UV 210 nm; retention times: 18.3 min, 20.1 min, *ee* = 83%. Literature data for (*R*)-enantiomer[27] $[\alpha]_D^{25}$ +3.3 (c 1, $CHCl_3$) for 93% *ee* ^{1}H NMR corresponded to the lit data.[29]

Kinetic Measurements.

Determination of ε(1671cm^{-1}) for cyclohexenone (*MA*). To determine the ε of cyclohexenone at 1671 cm^{-1}, IR spectra of pure cyclohexenone in CH_2Cl_2 were recorded at concentrations of 0.268 M (c1) and 0.276 M (c2). On the basis of the equation D = εcl and obtained values of D1 = 0.6863, and D2 = 0.6907, values of ε1 (1671 cm^{-1}) = 413.5 and ε2 (1671 cm^{-1}) = 403.6 were calculated. The average value of ε = 408.6 was used for further calculations.

General procedure for kinetic experiments of the catalytic Michael reaction. To a solution of (*R*)-BIMBOL, PhOLi and cyclohexenone in anhydrous methylene chloride under argon in a thermostated flask, diethyl malonate was added. An aliquot was immediately taken to fill a cell (CaF_2, l = 0.062mm). IR spectra were then recorded with intervals of 3-5 minutes.

Methodology for ab-initio calculations. *Ab-initio* calculations were performed using the ORCA software suite[28] within a Density Functional Theory (DFT) framework. The PBE[29] functional with empirical correction for dispersion interactions to the total energy[30] was used for geometry optimisation, and PBE0[31] functional was used for single-point energy evaluation in optimised geometry, in combination with a def-4 basis set based on a loosely contracted triple-ζ def2-TZV basis.[32] Numerical approximations implemented in the ORCA suite (a dual-grid integration technique in DFT calculation, RI and RI-JK approximations) were used to speed up the calculations, as test calculations without these approximations yielded virtually the same energy differences.

Acknowledgements

Authors gratefully thank the financial support from RSF 15-13-00039 and RBFR 15-53-05014 grants.

Notes and references

‡ Crystallographic data for (*S*)-BIFOL×H_2O has been submitted to CCDC and given code CCDC 1409564.

1 For reviews see: '*Comprehensive Asymmetric catalysis, and Supplements 1 and 2*', E. N. Jacobsen, A. Pfaltz and H. Yamamoto Eds., Springer, New York, 1999; K. Ohmatsu and T. Ooi, *Tetrahedron Lett.*, 2015, **56**, 2043–2048; '*Introduction to Frontiers in Transition Metal Catalyzed Reactions*', J. A. Gladysz Ed., *Chem. Rev.,* 2011, **111**, 1167–2486; S. Matsunaga and M. Shibasaki, *Chem. Commun.*, 2014, **50**, 1044–1057.

2 For reviews see: M. Waser '*Progress in the Chemistry of Organic Natural Products. Asymmetric Organocatalysis in Natural Product Syntheses*', Springer, New York, 2012; R. Sutar and N. Joshi, *Tetrahedron: Asymmetry*, 2013, **24**, 1345–1363; A. Quintavalla, L. Cerisoli and E. Montroni, *Current Organocatalysis*, 2014, **1**, 107–171; A. Moyano and R. Rios, *Chem. Rev.*, 2011, **111**, 4703–4832; S. Shirakawa and K. Maruoka, *Angew. Chem. Int. Ed.*, 2013, **52**, 4312–4348; C. M. R. Volla, I. Atodiresei and M. Rueping, *Chem. Rev.*, 2014, **114**, 2390–2431; '*Asymmetric Organocatalysis*' *Top. Curr. Chem.*, 2009, **291** (Ed. B. List), Springer, New York; R. J. Phipps, G. L. Hamilton and F. D. Toste, *Nature Chem.*, 2012, **4**, 603–614.

3 S. Schenker, A. Zamfir, M. Freund and S. Tsogoeva, *Eur. J. Org. Chem.*, 2011, 2209–2222; T. Akiyama, *Chem. Rev.*, 2007, **107**, 5744–5758; A. G. Doyle and E. N. Jacobsen, *Chem. Rev.*, 2007, **107**, 5713–5743; J. Yu, F. Shi and L.-Z. Gong, *Acc. Chem. Res.*, 2011, **44**, 1156–1171; M. Mahlau and B. List, *Angew. Chem. Int. Ed.*, 2012, **51**, 2–18; D. Parmar, E. Sugiono, S. Raja and M. Rueping, *Chem. Rev.*, 2014, **114**, 9047–9153; T. J. Auvil, A. G. Schafer and A. E. Mattson, *Eur. J. Org. Chem.*, 2014, 2633–2646; C. Uyeda and E. N. Jacobsen, *J. Am. Chem. Soc.*, 2011, **133**, 5062–5075; H. B. Jang, H. S. Rho, J. S. Oh, E. H. Nam, S. E. Park, H. Y. Bae and C. E. Song, *Org. Biomol. Chem.*, 2010, **8**, 3918–3922; G.

View Article Online
DOI: 10.1039/C6CY01697A

Tarkanyi, P. Kiraly, T. Soos and S. Varga, *Chem. Eur. J.*, 2012, **18**, 1918–1922; Y. Fan and S. R. Kass, *Org. Lett.*, 2016, **18**, 188–191.
4 "Enzyme Catalysis in Organic Synthesis", P. T. Anastas and R. H. Crabtree Eds., Wiley-VCH, Stuttgart, 2009.
5 M. S. Taylor and E. N. Jacobsen, *Angew. Chem., Int. Ed.*, 2006, **45**, 1520–1543; Y. Yamaoka, H. Miyabe and Y. Takemoto, *J. Am. Chem. Soc.*, 2007, **129**, 6686–6687; S. J. Zuend and E. N. Jacobsen, *J. Am. Chem. Soc.*, 2007, **129**, 15872–15883; J.-F. Bai, L.-L. Wang, L. Peng, Y.-L. Guo, L.-N. Jia, F. Tian, G.-Y. He, X.-Y. Xu and L.-X. Wang, *J. Org. Chem.*, 2012, **77**, 2947−2953; A. Quintavalla, L. Cerisoli and E. Montroni, *Curr. Organocatalysis*, 2014, **1**, 107–171.
6 G. Jindal, H. Kisan and R. Sunoj, *ACS Catal.*, 2015, **5**, 480−503; J.-C. Wasilke, S. Obrey, R. Baker and G. Bazan, *Chem. Rev.*, 2005, **105**, 1001–1020.
7 T. T. Dang, F. Boeck and L. Hintermann, *J. Org. Chem.*, 2011, **76**, 9353–9361.
8 H. Yamamoto and K. Futatsugi, *Angew. Chem. Int. Ed.*, 2005, **44**, 1924–1942.
9 H. Sasai, T. Arai, Y. Satow, K. N. Houk and M. Shibasaki, *J. Am. Chem. Soc.*, 1995, **117**, 6194–6198; M. Shibasaki, M. Kanai, S. Matsunaga, N. Kumagai, *Acc. Chem. Res.*, 2009, **42**, 1117–1127; J. R. Robinson, J. Gu, P. J. Carroll, E. J. Schelter and P. J. Walsh, *J. Am. Chem. Soc.*, 2015, **137**, 7135–7144; R. Schiffers and H. Kagan, *Synlett*, 1997, 1175–1176; I. Holmes and H. Kagan, *Tetrahedron Lett.*, 2000, **41**, 7453–7456; M. Nakajima, Y. Orito, T. Ishizuka and S. Hashimoto, *Org. Lett.*, 2004, **6**, 3763–3765; T. Ichibakase, Y. Orito and M. Nakajima, *Tetrahedron Lett.*, 2008, **49**, 4427–4429; Y. Orito, S. Hashimoto, T. Ishizuka and M. Nakajima, *Tetrahedron*, 2006, **62**, 390–400; M. Hatano, T. Ikeno, T. Miyamoto and K. Ishihara, *J. Am. Chem. Soc.*, 2005, **127**, 10776–10777; M. Hatano, T. Horibe and K. Ishihara, *J. Am. Chem. Soc.*, 2010, **132**, 56–57; H. Yan, J. S. Oh, J. W. Lee and C. E. Song, *Nat. Commun.*, 2012, **3**, 1212; T. Otani, A. Sugawara and Y. Tamai, *Tetrahedron Lett.*, 2014, **55**, 4923–4926; S. Kotani, M. Moritani and M. Nakajima, *Asian J. Org. Chem.*, 2015, **4**, 616–618.
10 Y. N. Belokon, K. A. Kochetkov, T. D. Churkina, N. S. Ikonnikov, A. A. Chesnokov, O. V. Larionov, I. Singh, V. S. Parmar, S. Vyskoc˘il and H. B. Kagan, *J. Org. Chem.*, 2000, **65**, 7041–7048; Y. N. Belokon, Z. T. Gugkaeva, V. I. Maleev, M. A. Moskalenko, M. North and A. T. Tsaloev, *Tetrahedron: Asymmetry*, 2010, **21**, 1793–1796; Y. N. Belokon', V. I. Maleev, Z. T. Gugkaeva, M. A. Moskalenko, A. T. Tsaloev, A. S. Peregudov, S. Ch. Gagieva, K. A. Lyssenko, V. N. Khrustalev and A. V. Grachev, *Russ. Chem. Bull.*, 2007, **56**, 1507–1514; Y. N. Belokon, S. Harutyunyan, E. V. Vorontsov, A. S. Peregudov, V. N. Chrustalev, K. A. Kochetkov, D. Pripadchev, A. S. Sagyan, A. K. Beck and D. Seebach, Arkivoc 2004, iii, 132–150.
11 Y. N. Belokon, Z. T. Gugkaeva, V. I. Maleev, M. A. Moskalenko, A. T. Tsaloev, V. N. Khrustalev and K. V. Hakobyan, *Tetrahedron: Asymmetry*, 2011, **22**, 167–172.
12 G. Kagan, W. Li, D. Li, R. Hopson and P. G. Williard, *J. Am. Chem. Soc.*, 2011, **133**, 6596–6602; J. Liang, A. C. Hoepker, A. M. Bruneau, Y. Ma, L. Gupta and D. B. Collum, *J. Org. Chem.*, 2014, **79**, 11885−11902; K. J. Jin, and D. B. Collum, *J. Am. Chem. Soc.*, 2015, **137**, 14446–14455.
13 N. T. Tran, S. O. Wilson and A. K. Franz, *Org. Lett.*, 2012, **14**, 186–189.
14 Q. Wang, X. Chen, L. Tao, L. Wang, D. Xiao, X.-Q. Yu and L. Pu, *J. Org. Chem.*, 2007, **72**, 97–101.
15 T. H. Siddall and W. E. Stewart, *J. Org. Chem.*, 1969, **34**, 233–237; W. T. Ford, T. B. Thompson, K. A. J. Snoble and J. M. Timko, *J. Am. Chem. Soc.*, 1975, **97**, 95–101.
16 C. Yang, X.-S. Xue, X. Li and J.-P. Cheng, *J. Org. Chem.*, 2014, **79**, 4340−4351.
17 W. N. Olmstead and F. G. Bordwell, *J. Org. Chem.*, 1980, **45**, 3299–3305.
18 R. F. W. Bader, '*Atoms In molecules. A Quantum Theory*', Clarendron Press, Oxford, 1990.
19 E. Espinosa, E. Molins and C. Lecomte, *Chem. Phys. Lett.*, 1998, **285**, 170–173; E. Espinosa, I. Alkorta, I. Rozas, J. Elguero, E. Molins, *Chem. Phys. Lett.*, 2001, **336**, 457–461.
20 J. M. Mayer, *Acc. Chem. Res.*, 2011, **44**, 36–46; J. Bonin, C. Costentin, M. Robert, J.-M. Savéant and C. Tard, *Acc. Chem. Res.*, 2012, **45**, 372–381.
21 Q. Wang, X. Chen, L. Tao, L. Wang, D. Xiao, X.-Q. Yu and L. Pu, *J. Org. Chem.*, 2007, **72**, 97–101.
22 Y.-L. Zhang and Q.-H. Fan., *J. Chem. Res. (S)*, 2005, 778–779.
23 X. Li, Q. Ding, J. Ge, J. Xie and D. Xu, *J. Org. Chem.*, 2009, **74**, 1785–1787.
24 D.-W. Wang, S.-M. Lu and Y.-G. Zhou, *Tetrahedron Letters*, 2009, **50**, 1282–1286.
25 Y. Yao, H. Shu, B. Tang, S. Chen, Z. Lu and W. Xue, *Chin. J. Chem.*, 2015, **33**, 601–609.
26 K.-X. Xu, L.-R. Yang, Y.-X. Wang, J. Zhao and C.-J. Wang, *Supramol. Chem.*, 2010, **22**, 563–570.
27 V. Waschol owski, R. K. Knudsen, E. T. C. Mitchell and V. S. Ley, *Chem. Eur, J.*, 2008, **14**, 6155–6165.
28 F. Neese and F. Wennmohs, '*ORCA - An Ab Initio, DFT and Semiempirical SCF-MO Package*' 2014.
29 A. D. Becke, *J. Chem. Phys.*, 1993, **98**, 5648–5652.
30 J. P. Perdew, K. Burke and M. Ernzerhof, *Phys. Rev. Lett.*, 1996, **77**, 3865–3868.
31 C. Adamo and V. Barone, *J. Chem. Phys.*, 1999, **110**, 6158–6170.
32 F. Weigend and R. Ahlrichs, *Phys. Chem. Chem. Phys.*, 2005, **7**, 3297–3305.

GRAPHICAL ABSTRACT